



Tectonics

RESEARCH ARTICLE

10.1029/2017TC004798

Key Points:

- New seismic reflection, and borehole data from the Danakil Depression, Ethiopia, constrains late-stage continental breakup
- A thick sequence of evaporites has been deposited over tens to hundreds of thousands of years in a basin bounded by a major, E-dipping normal fault
- The onset of magmatic extension during continental rift development does not necessarily herald the onset of seafloor spreading

Supporting Information:

- Supporting Information S1

Correspondence to:

I. D. Bastow,
ibastow@ic.ac.uk

Citation:

Bastow, I. D., Booth, A. D., Corti, G., Keir, D., Magee, C., Jackson, C. A.-L., et al. (2018). The development of late-stage continental breakup: Seismic reflection and borehole evidence from the Danakil Depression, Ethiopia. *Tectonics*, 37, 2848–2862. <https://doi.org/10.1029/2017TC004798>







Received 11 SEP 2017

Accepted 19 JUL 2018

Accepted article online 1 AUG 2018

Published online 6 SEP 2018

The Development of Late-Stage Continental Breakup: Seismic Reflection and Borehole Evidence from the Danakil Depression, Ethiopia

Ian D. Bastow¹ , Adam D. Booth² , Giacomo Corti³ , Derek Keir^{4,5} , Craig Magee¹ , Christopher A.-L. Jackson¹ , John Warren⁶, Jason Wilkinson⁷, and Matteo Lascialfari²

¹Department of Earth Science and Engineering, Imperial College London, London, UK, ²Institute of Applied Geoscience, School of Earth and Environment, University of Leeds, Leeds, UK, ³Consiglio Nazionale delle Ricerche, Istituto di Geoscienze e Georisorse, Florence, Italy, ⁴Ocean and Earth Science, University of Southampton, Southampton, UK, ⁵Dipartimento di Scienze della Terra, Università degli Studi di Firenze, Florence, Italy, ⁶Department of Geology, Chulalongkorn University, Bangkok, Thailand, ⁷Allana Potash Corporation, Addis Ababa, Ethiopia

Abstract During continental breakup, the locus of strain shifts from a broad region of border faulting and ductile plate stretching to a narrow zone of magma intrusion in a young ocean basin. Recent studies of volcanic rifts and margins worldwide suggest this shift occurs subaerially, before the onset of seafloor spreading. We test this hypothesis using recently acquired seismic reflection and borehole data from the Danakil Depression, Ethiopia, a unique region of transition between continental rifting and seafloor spreading. Our data, located near Dallol, ~30 km northwest of the Erta’Ale Volcanic Segment, reveal a remarkably thick (>1-km) sequence of young (~100-ka) evaporites in a basin bound by a major (≤400-m-throw), east-dipping normal fault. To generate such a large amount of subsidence in such a relatively short time, we propose that upper-crustal extension in Danakil is currently dominated by faulting, not magmatic intrusion. Given the region’s markedly thinned crust (~15-km-thick), relative to elsewhere in Afar where magma-assisted rifting dominates and maintains crustal thickness at ~25 km, mechanical extension in Danakil is likely coupled with ductile extension of the lower-crust and mantle lithosphere. Despite proximity to the voluminous lavas of the active Erta’Ale Volcanic Segment, evidence for igneous material in the upper ~2 km of the 6- to 10-km-wide basin is limited. Late-stage stretching was likely aided by thermal/strain-induced lithospheric weakening following protracted magma-assisted rifting. Basin formation immediately prior to the onset of seafloor spreading may also explain the accumulation of thick marine-seepage-fed evaporite sequences akin to those observed, for example, along the South Atlantic rifted margins.

1. Introduction

1.1. Overview

During continental breakup, the locus of extension is expected to shift from broad (~80-km-wide) regions dominated by long (>60-km), large-offset (>1-km) border faults to narrow (~20-km-wide), elongate (~60-km) zones of focused dike intrusion (e.g., Ebinger et al., 2017; Ebinger & Casey, 2001; Hayward & Ebinger, 1996). These narrow segments of magma-assisted rifting, which occur without marked crustal thinning (e.g., Mackenzie et al., 2005; Maguire et al., 2006) or subsidence (e.g., Rubin, 1992), are considered to delineate the final breakup plate boundary and herald the development of mid-ocean ridge spreading centers (e.g., Ebinger & Casey, 2001; Hayward & Ebinger, 1996; Keranen et al., 2004). Elucidating the processes controlling the transition from upper-crustal faulting, which is coupled with ductile plate stretching and thins the lithosphere, through to magma-assisted rifting and rupture, is therefore central to our understanding of the breakup process. This transition from mechanical (i.e., faulting and ductile plate stretching) to magma-dominated extension, and eventually breakup, is primarily preserved in the geological record along volcanic passive margins (e.g., Symonds et al., 1998; White et al., 2008). However, it is typically difficult to reconstruct the high-resolution spatial and temporal evolution of continental breakup from these volcanic passive margins because (i) their geology is only imaged using geophysical techniques (e.g., seismic reflection data); (ii) the tectonic-stratigraphic expression of incipient ocean crust development is deeply buried beneath thick post-rift sediments and volcanics, and is thus relatively poorly imaged (e.g., McDermott & Reston, 2015; Pickup et al., 1996; Ranero & Pérez-Gussinyé, 2010; Reeve et al., 2016; Reston, 2009; Reston & McDermott,

©2018. The Authors.

This is an open access article under the terms of the Creative Commons Attribution License, which permits use, distribution and reproduction in any medium, provided the original work is properly cited.

2014); and (iii) the tectonic and magmatic processes that acted during margin formation have long-since ceased and must therefore be inferred from the geological record.

Ethiopia is an ideal locale to study processes controlling the transition from mechanical to magma-assisted extension because it exposes several regions of asynchronous rift-sector development, from embryonic continental rifting in the south to incipient oceanic spreading further north in the Red Sea (Figure 1, e.g., Hayward & Ebinger, 1996). A consensus has emerged from a variety of disciplines that extension in much of the East African and Red Sea rift systems of Ethiopia is accommodated primarily by dike intrusion along narrow, magmatic segments, as opposed to border faulting and ductile plate stretching (e.g., Ebinger & Casey, 2001). Interferometric Synthetic Aperture Radar (InSAR) data provide the most unambiguous evidence for magma-assisted rifting in Ethiopia. Numerous hours-to-days duration dike intrusions into the middle and upper crust have now been documented in magmatic segments over the last two decades (e.g., Grandin et al., 2011; Keir et al., 2011; Wright et al., 2006). A plethora of data from Ethiopia also indicate that the magmatic segments are underlain by seismically fast (e.g., Keranen et al., 2004; Mackenzie et al., 2005), dense (Cornwell et al., 2006; Lewi et al., 2016) crustal bodies, interpreted to be gabbroic intrusions, with little evidence for crustal thinning (Mackenzie et al., 2005; Maguire et al., 2006). In conjunction with studies of lithospheric mantle structure (e.g., Bastow et al., 2010; Kendall et al., 2006), geodetic data overall point toward a model of extension in which final plate separation occurs by melt intrusion and not ductile stretching (e.g., Bilham et al., 1999; Wright et al., 2006).

Recent studies in the Danakil Depression of northern Afar have, however, challenged the view that a protracted period of magmatic extension via dike intrusion transitions smoothly into oceanic spreading (Bastow & Keir, 2011; Keir et al., 2013; Stab et al., 2016). Instead, the presence of markedly thinned Danakil crust, revealed by wide-angle seismic data, coupled with subsidence and deposition of Pliocene-to-Recent age evaporitic sedimentary rocks (Atnafu et al., 2015; Bonatti et al., 1971; Holwerda & Hutchinson, 1968; Lalou et al., 1970), suggests that the final stages of continental breakup may be characterized by an abrupt, late phase of ductile plate stretching and associated upper crustal mechanical extension (Bastow & Keir, 2011; Keir et al., 2013). Such late-stage stretching, which would enhance decompression melting, may also explain why there is an increase in the volume of young basalt flows in the Erta'Ale Volcanic Segment (EAVS). While a late phase of stretching and subsidence is conceptually appealing, constraints on the upper-crustal subsurface structure in the Danakil Depression are lacking and wide-angle seismic refraction data do not carry the short length-scale information required to test the role of mechanical versus magmatic extension. To address this issue, we present a three-dimensional analysis of the subsurface structure of the northern end of the Danakil Depression sedimentary basin using reflection seismic data and accompanying core and well-log records from ~120 boreholes (Figure 2), acquired for industrial potash exploration between 2010 and 2013 (Figure 3). These new data offer a unique insight into the anatomy of a young sedimentary basin, forming sub-aerially during the final stages of continental rifting.

1.2. Tectonic-Stratigraphic Overview

The Danakil Depression lies at the northern end of the Afar region in north Ethiopia; this position marks the triple junction between the Nubian, Somalian, and Arabian plates, as well as the Danakil microplate, which are diverging due to extension in the Red Sea, Gulf of Aden, and East African rifts (Figure 1, e.g., Stab et al., 2016; Tesfaye et al., 2003). Present-day opening across the southern Red Sea rift is constrained by a relatively high density of GPS measurements (e.g., ArRajehi et al., 2010; Kogan et al., 2012; McClusky et al., 2010). These geodetic data show that north of 16°N, extension is entirely accommodated in the main Red Sea rift, spreading at ~15 mm/year. To the south of 16°N, the rift bifurcates into two branches: the main Red Sea and the subaerial Red Sea rift in Afar (i.e., the Danakil; Figure 1). Partitioning of extension between rift branches varies along strike, with the rate of extension increasing southward in Afar from around ~10 mm/year in the north in our study region to ~20 mm/year further south at ~13°N (McClusky et al., 2010; Vigny et al., 2006).

On the Nubian plate, Afar is separated from the high-elevation (2- to 3-km) Ethiopian plateau by ~60-km-long border faults that developed during the onset of Red Sea rifting at ~30 Ma (e.g., Stab et al., 2016; Wolfenden et al., 2005). Wide-angle seismic refraction surveys, coupled with teleseismic receiver functions, constrain the crustal thicknesses to be (i) ~15 km thick beneath the Danakil Depression, (ii) ~40–45 km thick beneath the Ethiopian plateau, (iii) ~25–30 km thick beneath the Danakil microplate, and (iv) ~25 km thick beneath most of central and southern Afar (Hammond et al., 2011; Maguire et al., 2006; Makris & Ginzburg, 1987; Stuart et al., 2006).

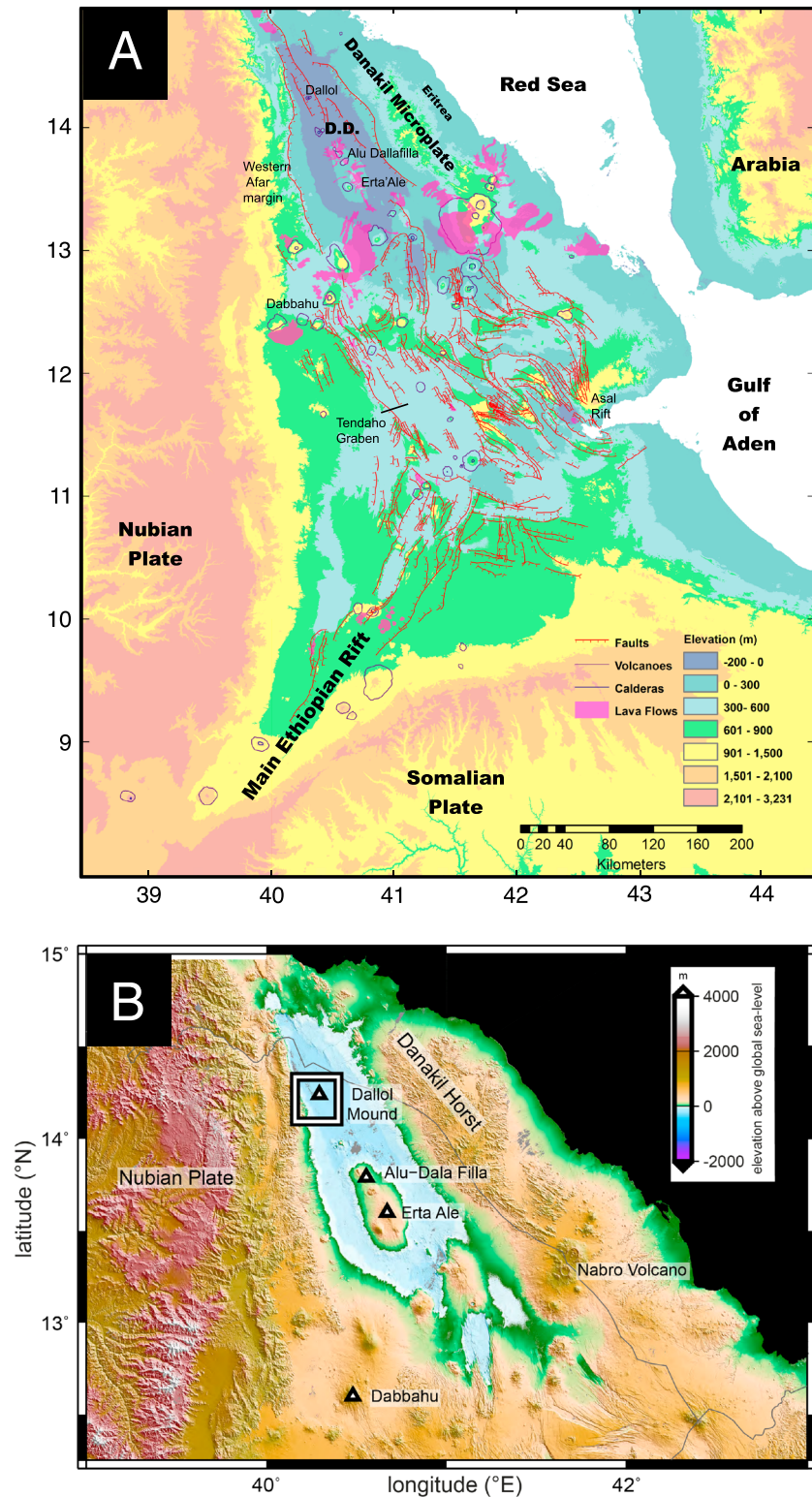


Figure 1. Location. (a) Topographic and structural map of the Afar depression modified after Keir et al. (2013). Major Pliocene-Recent faults are marked red. Recent basaltic lava flows are shaded light purple. (b) Regional tectonic setting of the Danakil Depression, Ethiopia. The square around Dallol Volcano delineates the main study area shown in Figure 2.

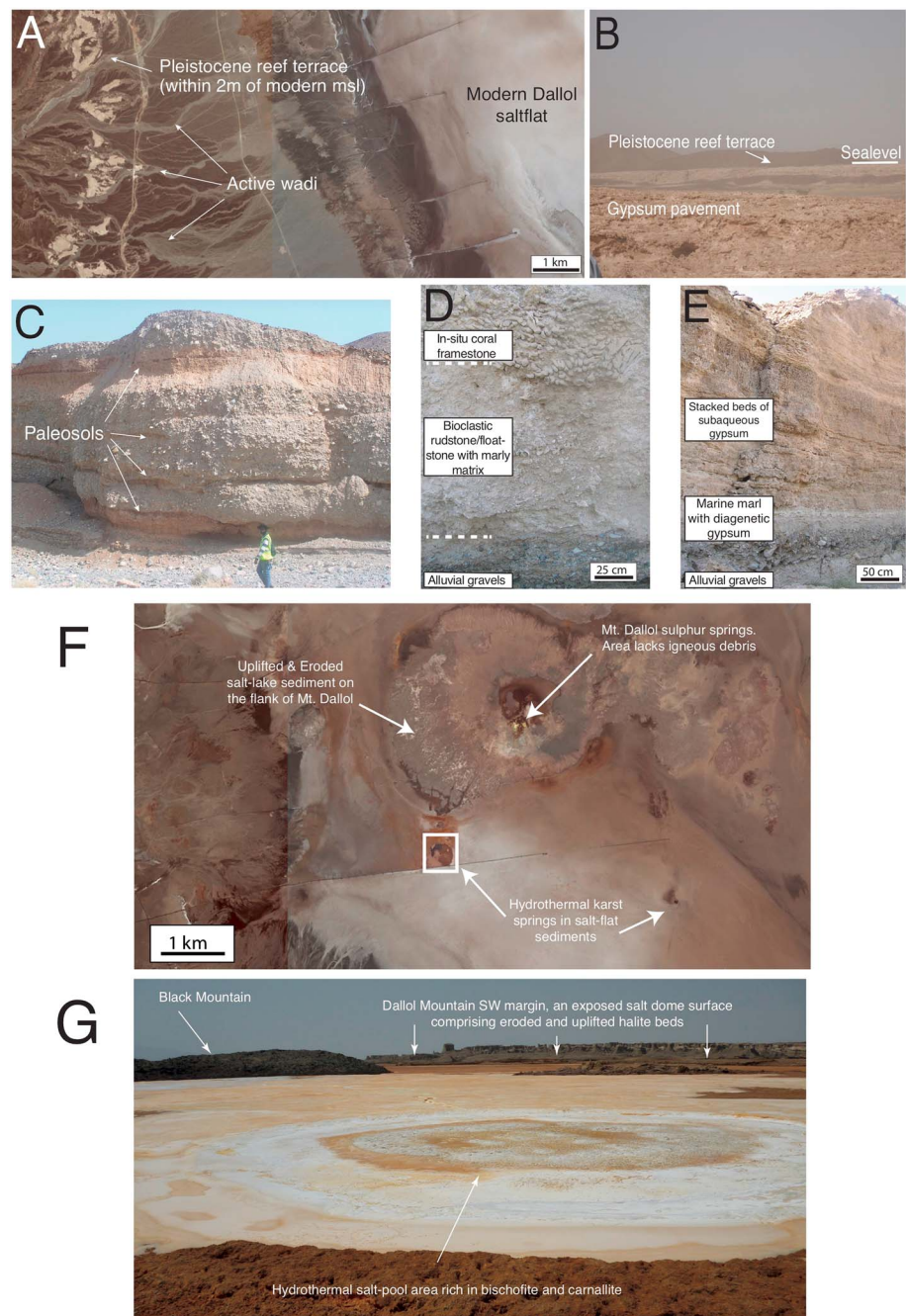


Figure 2. Surface geology of the Dallol Depression, Ethiopia. (a) Plan view of western margin showing the top of the gypsum pavement and outcrop of Pleistocene reef rim (image from Google Earth). (b) View from the eastern edge of the modern Dallol salt flat showing the subhorizontal benches that define former higher lake levels related to the of the subaqueous gypsum pavement and the even higher Pleistocene reef rim, which, where exposed around the edge of the Dallol Depression, lies within 2 m of current sea level (see Figure 2a for plan view), after Warren (2016). (c) Eroded cut along the edge of a wadi channel, showing stacked nature of wadi outflow gravels, separated by paleosols. (d) Reef rim geology showing in situ positions of a coral mass and the underlying wadi gravels, after Warren (2016). (e) Gypsum pavement composed of bottom-nucleated growth aligned forms of subaqueous gypsum that sits atop flat-lying marine marls (reef-equivalent) and underlying wadi gravels. (f) Regional overview of Dallol Mountain and salt flat; white rectangle shows the position of Black Mountain Lake where rising hydrothermal brines have dissolved the more soluble portions of the uplifted potash-entraining evaporite sediments that underlie Dallol Mountain (image from Google Earth). (b) Black Mountain Lake. View north across this active hydrothermal spring, with the southwest edge of the domed bedded sediments of Dallol Mountain on the horizon. Midground shows the pond area with carnallite, bischofite, and halite precipitates. Black Mountain Lake was the site where a hydrothermal crater formed in 1926.

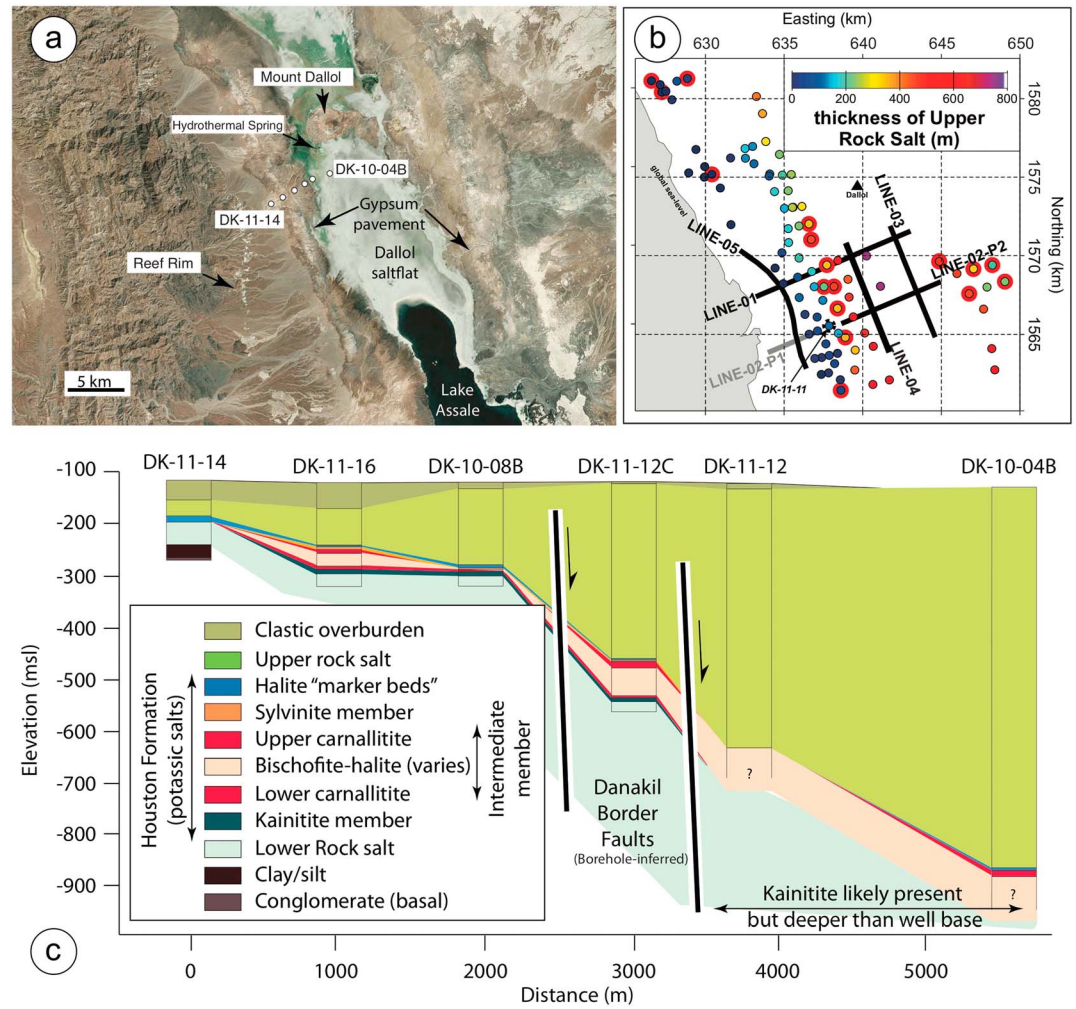


Figure 3. Borehole stratigraphy along seismic profile LINE-01. (a) Satellite image showing borehole positions and relevant surface geology features described in the text (image from Google Earth). (b) The Allana borehole data set, showing thickening evaporite sequences over the Danakil border faults. Circles are borehole locations, with colors indicating the thickness of the Upper Rock Salt. Log interpretations from borehole DK-11-11 and others as labeled, rock types are detailed further in Figure 4. Only the boreholes enclosed in red circles contain minor igneous material (typically ashfall tuff). Black/gray lines are the locations of seismic reflection profiles. (c) The geological cross section (depth in meters) that gives borehole control to the seismic interpretation along LINE-01 (see text for details).

Active volcanism within the Danakil Depression is generally confined to the EAVS, where it is characterized by basaltic lavas (Hagos et al., 2016) fed by relatively shallow-level (1- to 2-km-deep) magma reservoirs (Field et al., 2012; Magee et al., 2017; Nobile et al., 2012; Pagli et al., 2012). For example, in 2008, a basaltic eruption likely fed by a dyke tapping a saucer-shaped sill occurred at the Alu-Dalafilla volcanic center (Figure 1), ~40 km south of our study region (Magee et al., 2017; Pagli et al., 2012). On the strength of remote sensing mapping and InSAR data (Pagli et al., 2012), Magee et al. (2017) infer this eruption was fed by a shallow (~1-km-deep) saucer-shaped sill. Evidence for ongoing magma intrusion in our study area comes primarily from InSAR measurements that, in October 2004, documented the intrusion of a NW-striking (N155°E-striking), 9-km-long, ~0.06-km³ dike intruded laterally southwards from a 2.4-km-deep magma reservoir beneath Dallol (Figure 1; Nobile et al., 2012). Dike emplacement may have been associated with slip on an adjacent N-striking (170–350°), east-dipping (58°) fault, which modeling suggests extends to shallower levels (<1 km depth) than the 2- to 6-km-depth range of the dike (Nobile et al., 2012). This phase of intrusion also triggered an Mw 5.5 earthquake on a normal fault ~3 km SW of our study area (Nobile et al., 2012).

1.3. Stratigraphic Overview

Pleistocene–Recent evaporites are widespread in the Danakil Depression (e.g., Bonatti et al., 1971; Foubert et al., 2018; Garland, 1980; Lalou et al., 1970), where they may occasionally be covered by a thin veneer (<50 m thick) of clastic sedimentary rocks. Today, the Dallol salt flat, a halite-floored elongate salt pan, occupies the central part of the northern Danakil Depression and forms a basin covering 400 km² (Figure 1b). The salt pan's position is asymmetric within the Danakil Depression; it lies near the western edge of the basin, ~5 km from the foot of the escarpment to the Ethiopian Highlands, but ~50 km from the eastern margin of the depression in Eritrea. The Dallol salt pan and adjacent Lake Assele today constitute the deepest continental drainage sump in Afar, with the surface of the pan being ~116 m below sea level (Figures 1 and 3a). The flat area located east and northeast of the main modern Dallol salt pan is mostly an extensive gypsum plain (Bannert et al., 1970).

The surface geology of the Dallol salt pan comprises four depositional associations and terraced outcrop belts (Figure 2a): (1) the saline pan halite crusts and layers of the pan center, (2) gypsum beds outcropping in the pavement area, (3) a marine reef rim, and (4) alluvial sediments making up the Bajada rim (Figures 2a–2c). Alluvial sediments underlie and crosscut the reef rim and gypsum pavements, interfingering laterally with the halite-dominated beds of the depression center (Figures 2d and 2e).

The curvilinear outcrop trace of the Pleistocene reef rim roughly defines a level in the basin that is within a few meters of modern sea level and records the last marine incursion into the basin (Figures 2a and 3a). The reef rim and associated stromatolites date between Marine Isotope Stage (MIS) 7 (~240 ka) and MIS 5e (~120 ka; Foubert et al., 2015a, 2015b). Latter stages of the coralgall reef terrace growth indicate that normal marine water was last present in the basin ~120 ka. Like the reef rim, the gypsum pavement fringe defines a consistent elevation level or surface, most clearly visible along the western margin of the present salt flat (Figure 2b). Sediments of the stratiform gypsum pavement are consistent with a former arid marine-seepage lake hydrology defined by a water surface at lower elevation than the reef rim, beginning soon after the marine connection to the basin was lost and stabilizing ~80 m below sea level (Figure 2b). Waters supplying both the reef rim and the gypsum unit had a predominantly marine source, the former with a surface connection to Red Sea, the latter via a marine seepage feed.

The ephemeral salt pan hydrology active today in the lowest parts of the Dallol salt flat is depositing a stack of bedded salt crusts, interbedded with clay layers. The clays are carried into the depression via occasional sheetfloods, followed by desiccation of the surface waters as the clays flocculate and settle; salinities then increase to halite saturation, and salt crusts composed of aligned halite chevrons are deposited on a modern pan surface that is ~116 m below sea level (Figure 2a; Warren, 2016). This ephemeral brine flat hydrology is stable with respect to the current climate (groundwater inflow ≈ outflow). The current brine flat of the northern Danakil Depression is therefore accumulating bedded pan salt at an even lower topographic level in the basin than the surrounding gypsum pavement, implying that modern halite-dominant pan beds form under more arid conditions (less humid, more drawdown) than those of the gypsum pavement (Warren, 2016).

Pleistocene–Recent evaporites are widespread in the Danakil Depression (e.g., Bonatti et al., 1971; Garland, 1980; Lalou et al., 1970), where they may occasionally be covered by a thin veneer (<50 m thick) of clastic sedimentary rocks. Whilst the surface geology suggests deposition in the Danakil Depression around Dallol has progressed from a marine environment ~120 ka to an arid environment, it is difficult to constrain the regional subsurface sedimentology and stratigraphy due to a lack of rock outcrop. We overcome this evidential gap by combining observations of surface geology with ~120 borehole logs and 2-D seismic reflection profiles from the area. These data sets are reviewed in the following sections.

Despite the widespread view that the Mount Dallol is an igneous feature (e.g., Nobile et al., 2012), there are no observable surficial volcanic products (lava, ashfall, or scoria) on or near it (Figure 2f). This is the case even in the region of the most recent phreatic activity at “Black Mountain” (Figure 2g), where in 1926 a 30-m-diameter phreatic crater formed in salt beds (Figure 2g; Siebert et al., 2010). All the rocks associated with this cavity and its formative event at the pan surface are nonvolcanic, suggesting that Dallol mountain's formation mechanism differs from the magmatic events that created the volcanoes along the EAVS. Instead, the Dallol mountain crest comprises uplifted and eroded halite and potash beds soaked in a hydrothermal hydrology that emerges on the lake surface as several hot, bubbling, sulfurous brine pools (Figure 2f).

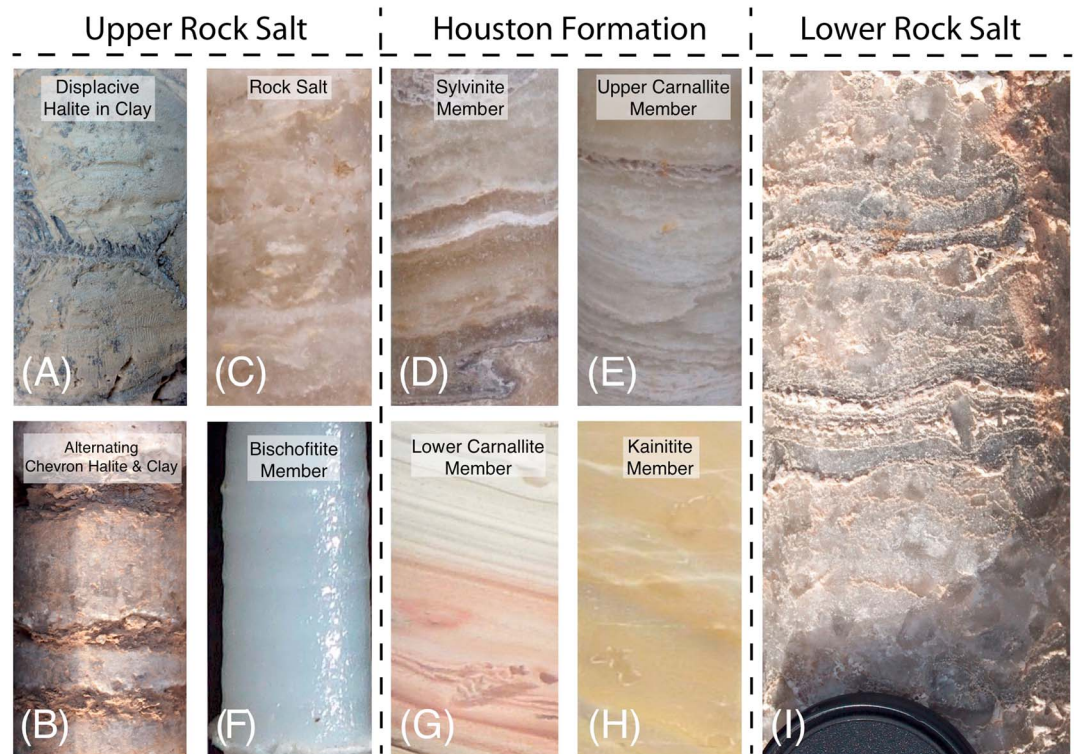


Figure 4. Representative core examples of the various units that make up the evaporite units in the Danakil Depression (see Figure 3c for a stratigraphic breakdown). Modified after Warren (2016).

2. Borehole Geology of the Dallol Area

Well-log data from ~120 boreholes, which sample evaporites as deep as 966 m below the Dallol salt pan, allow the nature and composition of evaporitic sediments filling the upper part of the Danakil Depression (Figures 3 and 4) to be constrained. These data reveal that the basin contains an upper, clastic-dominated sequence that is only penetrated by boreholes on the western basin margin (e.g., DK-11-14; Figure 3b). Three large-scale evaporite units are intersected in boreholes located away from the basin margin. From top to bottom these evaporite units are (Figures 3c and 4): (1) Upper Rock Salt (URS); (2) Houston Formation, which is potash rich and extensively mined; and (3) Lower Rock Salt (LRS). Application of standard cross-plotting techniques, comparing gamma and density logs (Hill, 1993), allows separation in all available boreholes of (i) the potassic Houston Formation from the surrounding salt units and (ii) the LRS from the nonpotassic and porous URS (Figures 3b and 3c).

The LRS is >500 m thick and dominated by bottom-growth-aligned, subaqueous halite textures. Unlike the URS, it lacks significant levels of siliciclastic detritus (Figure 4i). Halite textures in the LRS lack porosity and are dominated by coarsely crystalline beds comprising centimeter-scale NaCl-CaSO₄ couplets, dominated by upward-pointing halite chevrons, mantled by thin CaSO₄ layers (Warren, 2016). This meromictic-holomictic textural association passes up into the upper part of the LRS with centimeter-scale proportions of alternating less- to more-saline episodes of evaporite precipitation. This alternation decreases upwards, indicating an overall increasingly shallow subaqueous depositional setting toward the base of the Kainite Member that defines the base Houston Formation (Warren, 2016).

Between the URS and LRS, the 15- to 40-m-thick Houston Formation has been drilled and cored extensively (Figure 3c). Stratigraphically, the Houston Formation comprises several members (Figure 4), which are variably present within the Dallol salt pan. The Kainite Member (4–14 m thick, Figure 4h), which passes down in depositional continuity with the LRS, contains ≤50% kainite cumulates in a cumulate halite (nonchevron) background. Above this are the Carnallite Members (Figures 4e and 4g), between which the Sylvinite Member

(0–10 m thick) is variably deposited. Where present, the upper part of the Carnallite unit commonly displays evidence for dissolution and reprecipitation.

In parts of the evaporite unit nearer to the western side of the basin, thick bischofite intervals (Figures 3 and 4) separate the carnallite units. The bischofite is layered at a millimeter-to-centimeter scale, with no obvious breaks related to freshening and exposure, suggesting that it was deposited in a perennially subaqueous or phreatic cavity setting (Warren, 2016). The potash/bischofite interval passes up into a slumped and disturbed halite-dominated unit that contains clay lamina termed the *Marker Beds*. The top of the Marker Beds corresponds to an unconformity, on to which the URS was deposited.

Textures and mineralogies in the URS define a separate hydrological association to the marine-fed LRS and Houston Formation: They are like those forming in and beneath the modern salt pan surface (Figures 2c and 2d; Warren, 2016). The URS, especially its upper part, shows textural evidence of periodic and ongoing clastic-rich sheet-flooding and freshening (Figure 4). These textural observations imply deposition occurred in a perennial to pan hydrology akin to today's halite pan surface (cf. Lake Asal, Djibouti; Figure 1; Warren, 2016). The URS is interpreted as having formed rapidly in a sequence passing from near-pure subaqueous lacustrine halite to pan halites with higher levels of clay sheetflood influx. At the western margin of the study area, the URS is typically <50 m thick (Figures 3b and 3c). Superimposed onto a gradual thickening of the URS eastwards are two abrupt changes in thickness, each up to ~200 m, which occur between boreholes DK-10-08B–DK-11-12C and DK-11-12C–DK-11-12 (Figure 3b). The location and extent of the abrupt thickening eastwards of the URS is constrained by the closely spaced array of boreholes and appears to trend NW-SE (Figure 3b); we interpret that these thickness patterns define two NW-striking, E-dipping, normal faults. The thickest part of the URS is toward the center of the Dallol salt pan; borehole DK-10-04B (Figure 3a), for example, shows 400–500 m of nonpotassic URS salt accumulated in <120 ka ($\approx 4\text{--}5$ mm/year).

Above and lateral to the URS is a clastic unit with significant amounts of lenticular gypsum and displacive halite, which occasionally dominate. The unit thickens toward the margins of the basin (Figure 3c). The widespread presence of diagenetic salts in a clay host indicates high pore salinities as, or soon after, the saline beds that stack into the clastic unit were deposited (Figure 4a; Warren, 2016).

Igneous rocks are only sparsely intersected by the potash-entraining boreholes (Figure 3), despite the proximity to the EAVS. Evidence for an igneous association is restricted to sporadic, thermally altered evaporites and occasional tuff/ashfall deposits. The latter show neither consistent depth nor stratigraphic position beyond their restricted occurrence in the upper 200 m and are possibly related to eruptions at Erte'Ale. In borehole DK-11-38 (Figure 3), ~22 m of basalt/dolerite appears at ~170 m depth within and concordant to the layering in the evaporite host rock. Absent from all other boreholes, this body likely represents a localized lava flow or sill.

The lack of extrusive igneous rocks on or around Dallol Mountain does not preclude the feature being a response to emplacement of underlying magmatic material. For example, Nobile et al. (2012) showed that Mount Dallol is located near a yet-to-surface actively emplacing igneous dike (Figure 1). The Dallol Mountain could thus represent a salt dome, capped by phreatic cone/hydrothermal karst structures, generated in response to the migration and stalling of molten magma at depth (i.e., an intrusion-induced forced fold; Magee et al., 2017; Pollard & Johnson, 1973).

2.1. Seismic Reflection Data

We interpreted four 2-D, prestack time-migrated seismic reflection profiles, acquired in 2010 by TESLA-IMC, and have mapped nine seismic horizons (A-I), and several normal faults were mapped (Figure 5). In the absence of check shot surveys and/or sonic logs, borehole formation depths are converted to seismic travel time using processing (stacking) velocities. The use of these, and the subsequent prestack Kirchhoff time-migration, contributes some error but prominent reflections in the seismic data tie to within ± 5 ms of prominent stratigraphic surfaces, and the mismatch in the well tie to the inferred base URS/top Houston Formation (Horizon C) is typically <20 m (Booth et al., 2011; Lascialfari, 2017). Such errors are insignificant compared to the bulk structure we interpret. Throughout the depth range of interest, the dominant frequency of seismic wavelets is consistently ~55 Hz. Because velocities increase from 2,500 to 4,750 m/s with depth, the implied wavelength of the seismic wavelet increases from 45 to 86 m. Assuming a one fourth-wavelength resolution criterion, horizons separated by 10–20 m should thus present discretely resolvable seismic reflections.

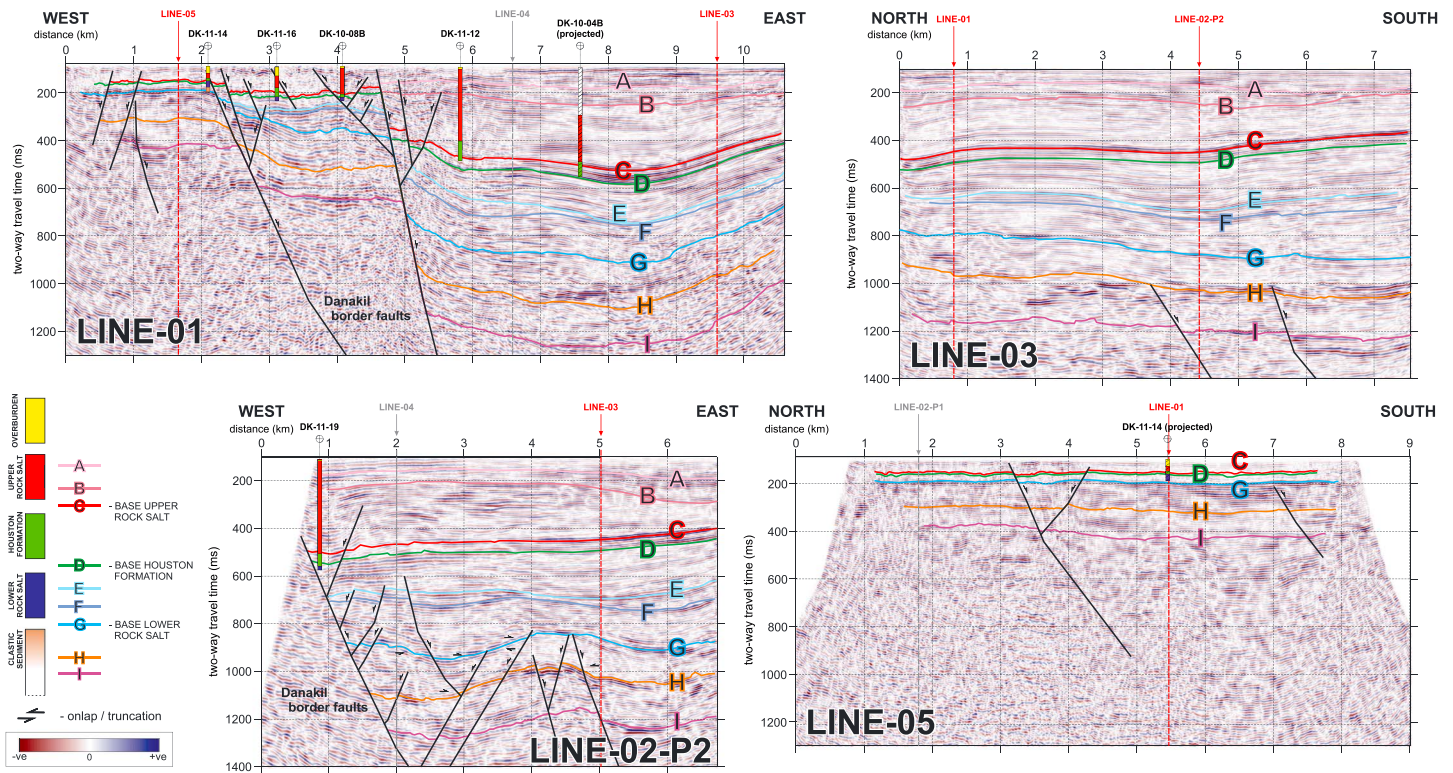


Figure 5. Interpreted seismic lines (i.e., LINE-01, LINE-03, and LINE-05) overlain by lithological summaries from intersecting or nearby projected boreholes. See Figure 2 for locations. Horizons C, D, and G are interpreted, respectively, as the bases of the URS, the Houston Formation and the LRS. Uninterpreted seismic lines are in the supporting information.

We mapped two major, NW-striking (~160–340°), E-dipping (~60°) normal faults that extend from the base of the seismic record and tip out just below the surface (Figure 5). Because the data are in seismic travel time, it is difficult to accurately determine the dip of these normal faults, although we assume the faults likely dip at ~60°. Fault throw increases downwards and reach ~500-ms two-way travel time (TWT) at Horizon I. The major normal faults are associated with smaller (throw <20 ms) antithetic and synthetic normal faults (Figures 1 and 6). We also observed two prominent east-striking faults, one dipping north and the other south, which extend from the base of the seismic record and show throws of 11 and 153 ms, respectively, at Horizon I (Figure 5). None of the mapped faults coincide with the east-dipping normal fault modeled by Nobile et al. (2012).

The mapped horizons are deepest within the hanging wall of the easternmost NW-striking fault; toward the eastern edge of the survey, all horizons become shallower (Figure 5). Reflections beneath Horizon H are broadly continuous but often display lateral variations in amplitude and small offsets, perhaps attributable to tuning effects (layers thinner than ~20 m), out-of-plane reflections, and/or small-scale faulting (Figure 5). Below Horizon I there is little-to-no evidence of lateral variations in stratal thickness, although imaging in the footwall of the major normal faults is potentially impeded by poor migration performance (Figure 5). In the immediate hanging walls of the major NW- and E-striking faults, stratal packages bound by Horizons G–I appear to thicken subtly toward the fault planes (e.g., Line-02-P2). Furthermore, the corresponding stratal package in the fault footwalls is typically ~<40-ms TWT thinner, implying that the faults were active

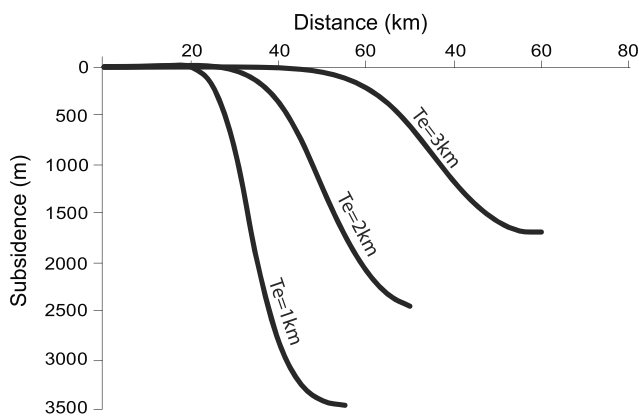


Figure 6. Plate deflection resulting from magma intrusion for different values of elastic thickness (T_e) of the lithosphere. Flexure is calculated for a single mafic intrusion with length 40 km, width 20 km, thickness 16 km, and a density contrast of 210 kg/m³. The Young's modulus and Poisson's ratio were 70 GPa and 0.30, respectively. Calculations include the additional load imposed by syn-rift sedimentation; we used a density of 2,380 kg/m³ for the sedimentary rocks, which were considered to completely fill the depression resulting from the intrusion-related flexure. Full details of the method used for the calculations are reported in Corti et al. (2015).

during deposition of these units (Figure 5). Both Horizons H and G truncate underlying reflections and are overlapped by overlying strata, demonstrating that they are erosional unconformities (Line-02-P2, Figure 5). Ties between borehole logs, particularly DK-11-14 (Figure 3), and seismic data indicate that Horizon G possibly marks the boundary between the overlying evaporite sequence and the early, clastic-dominated basin fill, but no well intersects this boundary in the outboard parts of the basin fill (Figure 5).

Above Horizon G, likely within the evaporite sequence, reflections are more continuous and display less lateral variation in amplitude compared to the underlying clastic-dominated basin fill (Figure 5). Within the basin center, east of the major faults, there is relatively little thickness variation between Horizons G and C (near the top of the Houston Formation), although some thickening of the Horizon G–F package is observed on Line-02-P2 (Figure 5). The lack of thickening of this package toward the east-dipping faults, coupled with onlap onto preexisting structural highs (i.e., footwall crests), suggests that the observed minor thickness variations are likely due to the infilling of topography as opposed to syn-kinematic deposition or salt flow (Figure 5). Horizons G–C thin across the easternmost NW-striking fault by ~280-ms TWT (Figure 5). The URS, bound by Horizons C–A, also thickens eastward across this fault, attaining a maximum thickness ~4 km east of the fault plane before thinning further east (Figures 4 and 6). This increased thickening of evaporite strata across the NW-striking faults, compared to that of the underlying clastic-dominated succession (i.e., Horizons I–G), implies that fault activity and creation of hanging wall accommodation increased during evaporite deposition. In places, Horizon B appears unconformable with underlying strata (Line 02-02, Figure 5).

Responses consistent with igneous material are absent throughout the seismic record. Typically, the seismic expression of an igneous body would include high-amplitude reflectivity preceding a region of extinguished signal, attributed to the weak transmission across the large acoustic impedance boundary (e.g., Fruehn et al., 2001; Magee et al., 2016; Petersen et al., 2006). An apparent reduction in the dominant frequency of the seismic energy, caused by scattering of high frequencies at the upper and internal boundaries of the body would also be expected to result from the presence of igneous material (e.g., Ziolkowski et al., 2003). Finally, a sequence of reverberations following the main response to the body, given a train of “interbed multiples” that become trapped within, would also be indicative of an igneous layer (e.g., Ziolkowski et al., 2003). Nowhere within the URS or LRS units are such expressions evident in the seismic data.

3. Discussion

3.1. Structural Style and Timing of Development of the Dallol Salt Pan

Seismic and borehole data indicate that the large-throw, east-dipping normal faults demarcate the boundary of a thick evaporite depocenter near Dallol in the northern Danakil Depression (Figure 5). Although our seismic sections do not cross the eastern side of the basin, the presence of gradually thinning sediments eastward suggests a full graben morphology, with the western faults being the most active and driving differential basin subsidence. The boundary of this evaporite-filled basin (i.e., the Dallol salt pan) is marked by sporadic outcrops of reefal carbonate rocks that predate the gypsum pavement, URS, and modern salt pan geology.

Seismic-stratigraphic observations allow us to determine the relative timing of fault activity within the Dallol salt pan. Minor thickness changes (~<40-ms TWT) in the Horizon I–G package across the major normal faults suggest these structures were active during deposition of the lower clastic sequence (Figure 5). Prominent thickening of the URS sequence across the main basin-bounding fault(s), as revealed by seismic (\leq ~260 ms; Figure 5) and borehole (up to ~700–800 m; Figures 3b and 3c) data, indicates deposition of this unit, and possibly the underlying evaporite units for which there is less borehole control, defines an abrupt increase in fault activity that facilitated rapid basin subsidence. Truncation of underlying reflections and onlap of overlying strata onto Horizon G indicate that this change in the rate of fault-driven subsidence is marked by the development of an unconformity (Figure 5).

The simplest interpretation of the origin of the Houston Formation is that it formed at the end of the most recent marine incursion into the Danakil, after which precipitation of a thick sequence of the URS began. Estimating the age of these marine deposits therefore constrains the maximum age of the last episode of drawdown. ^{230}U – ^{234}Th dating of corals and bivalves in reef rim carbonates flanking the basin (Foubert

et al., 2015a, 2015b) establishes that the last marine incursion into the Danakil Depression was 100–120 ka. We therefore consider that the maximum onset age of the last evaporite sequence is ~100 ka because the Horizon C unconformity, marking the base of the URS, represents a time gap of an unknown duration. To determine the extension history accommodating URS formation, we use an onset age for evaporite deposition of ~100 ka, the magnitude of displacement of throw of the URS (i.e., ~400 m, based on offset of the top of the Houston Formation in boreholes) across the major basin-bounding faults and assume faults dip at 60°, we estimate a long-term slip rate of ~5 mm/year. Because fault dip is uncertain, assuming dips of 50° or 70° would mean total extension ranges from 335 to 145 m and the long-term slip rate is 4.3–5.2 mm/year. If a conservative age (i.e., 120 ka) for the onset of URS deposition is considered, then a fault dip of 60° would correlate to a long-term slip rate of ~3.8 mm/year. These slip rates are consistent with long-term halite accumulation rates in many modern evaporite basins (Ruch et al., 2012; Warren, 2016), although short-term halite accumulation rates can approach 100 mm/year (Reading, 2009).

3.2. Formation of the Danakil Depression

Several processes could have generated accommodation for the evaporite-filled sub-sea-level drawdown Dallol salt pan in the Danakil Depression, including (i) tectonic faulting of the upper crust coupled with ductile stretching of the lower crust, (ii) dike intrusion-driven extension, or (iii) flexure due to the loading effects of dike intrusion. Our estimates of fault slip rate translate to an extension rate of ~2–3 mm/year, although we note that this rate would increase if the age of evaporite deposition is <100 ka. Estimates of current extension rate from GPS place are ~10 mm/year (McClusky et al., 2010). Assuming plate kinematics have not changed significantly in the last ~100 ka, our data place a lower bound estimate of 23% of extension accommodated by slip on this single fault. However, given that this estimate does not include faulting on the eastern side of the basin, or additional rift margin faults west of our seismic line, we consider that tectonic faulting of the upper crust likely dominates long-term upper crustal extension in this region.

While inversion of InSAR observations during the 2004 Dallol event (Nobile et al., 2012) suggests crustal dike intrusion triggered up to ~1 m of slip on a fault within the study area, its modeled position does not correspond directly to any of the faults we map but it could relate to one of our major basin-bounding faults. The observed displacements and length scales of faulting that we observe in the Dallol region (Figures 1 and 6) exceed those commonly associated solely with dike intrusion (~2 km, e.g., Dumont et al., 2016; Rowland et al., 2007). The combined magnitude, rate of fault slip, and amount of fault-related extension, coupled with the overall geometry of the basin, lead us to interpret that fault related extension, rather than dike intrusion extension dominate at least the northern portion of the Danakil Depression.

Length scales associated with the loading effects of diking also match poorly the observations from Dallol, that is, basin wavelength scales with effective elastic plate thickness (T_e), but even when T_e is small (e.g., ~4 km in Danakil; Ebinger & Hayward, 1996), the deformation zone produced by loading is expected to exceed the observed 6- to 10-km basin width of the basin by more than an order of magnitude (e.g., Corti et al., 2015). For $T_e < 4$ km, as may occur at mid-ocean ridges (e.g., Watts, 2001), the expected width of deformation (~60 km, even when $T_e = 1$ km) also exceeds the width of the Danakil Depression (Figure 6).

We suggest that tectonically driven, high-angle border faulting in the upper crust provides a simpler explanation for the observed basin geometry in Danakil, though we acknowledge, of course, that our present data set only samples a small portion of northern Danakil. However, our assertion is supported by observations of seismicity in the region, which show that over the last five decades of globally recorded seismicity, the western Afar margin border fault system next to the Danakil Depression has been characterized by higher seismic moment release than further to the south (Ayele et al., 2007; Keir et al., 2013). This distribution in seismicity implies that faulting in the Danakil Depression accommodates a larger proportion of extension than elsewhere in Afar. Additionally, local seismicity recorded in the Danakil during 2011–2013 shows that the in-rift fault system near Dallol is seismically active (Illsley-Kemp et al., 2017), consistent with the view that the role of magmatism in achieving extension here is reduced. To facilitate mechanical upper crustal extension and rapid basin subsidence, it is likely that contemporaneous ductile stretching of the lower crust and mantle lithosphere has occurred; this would explain the marked thinning of the crust in Danakil (~15 km) compared to elsewhere in Afar (~25 km; Bastow & Keir, 2011).

3.3. Implications for the Development of Continent-Ocean Transition in Afar

Previous studies of the Danakil Depression have confirmed that movement of Danakil relative to Nubia began ~11 Ma, with rifting being most intense since ~5 Ma (Eagles et al., 2002). Classic works from the 1970s had long since reported on the counterclockwise rotation of the Danakil Depression in the last several million years (Barberi & Varet, 1977). The onset of extension in Danakil is thus a relatively young phenomenon when compared to the ~30-Ma age of the Red Sea rift. The crust of the Danakil Depression is known to be continental in nature: A midcrustal discontinuity visible in wide-angle seismic data can, for example, be traced all the way back into the Main Ethiopian Rift and onto the Nubian plate (e.g., Maguire et al., 2006; Makris & Ginzburg, 1987). Seafloor spreading is thus not yet underway in the region. Compared to the distribution of shallow-marine reefal carbonates around the flanks of Danakil, which suggest extension across a relatively broad area, our seismic and borehole constraints support the hypothesis that a considerable portion of recent extension in the northern Danakil Depression has localized within a narrow (6- to 10-km-wide), evaporite-filled basin accommodated by faulting in the upper crust and ductile stretching of the lower crust and mantle lithosphere. Whilst geodetic observations indicate that ongoing dike intrusion occurs in the Danakil (e.g., Nobile et al., 2012; Pagli et al., 2012), the geometry of the evaporite-filled basin and thickness of sedimentary strata (>1 km) suggests intrusion is now likely subordinate to mechanical extension. The relative importance of mechanical extension is thus different to elsewhere in Afar, where rifting is magma-assisted and there is substantially thicker and fast seismic velocity crust despite similar amounts of total extension (e.g., Bastow & Keir, 2011; Dumont et al., 2016; Ebinger et al., 2010; Keir et al., 2015; Rooney et al., 2014; Rowland et al., 2007; Wright et al., 2006). The difference in extension style between Danakil and elsewhere in Afar implies that a late-stage shift in the mechanism of breakup has occurred in northern Ethiopia, after a phase of magma-assisted continental rifting, but prior to the onset of seafloor spreading.

Several observations could explain the onset of localized crustal stretching in the Danakil Depression during Pliocene times. North of ~13.5°N, where the rift floor extends toward and below sea level, the crust thins dramatically, T_e reduces to ~4 km, and the zone of active extension is closely flanked by both the Nubian plate and the Danakil microplate. Deformation on the Danakil microplate north of ~13.5°N is limited, and its geological record is dominated by Precambrian and Mesozoic rocks. The Danakil horst and Nubian plates may thus represent strong tectonic units that act to focus extension to a narrower region. Alternatively, heating of the crust in response to dike intrusion in the Quaternary-Recent magmatic segments is expected, even at the relatively slow extension rates observed in Afar, to weaken the crust on timescales of $\ll 1$ Ma and facilitate the onset of ductile deformation (e.g., Daniels et al., 2014). It is thus plausible that dike intrusion in the Danakil Depression during an earlier, buried and thus not imaged, magma-assisted rifting phase akin to that which is ongoing elsewhere in Afar, induced later ductile stretching and mechanical upper crustal extension phase, forming the Danakil Basin (Bastow & Keir, 2011). Whether the localization of strain is thermally or compositionally driven, our observations suggest that significant and relatively rapid normal faulting and associated accumulation of thick syn-rift packages of evaporites may occur during the final stages of continental breakup. The occurrence of ductile plate stretching and upper crustal mechanical faulting immediately prior to the onset of seafloor spreading in Danakil suggests that the resulting basin subsidence could accommodate deposition of thick evaporite sequences, like those observed along the South Atlantic rifted margins (e.g., Pickup et al., 1996; Ranero & Pérez-Gussinyé, 2010).

4. Conclusions

Seismic reflection data and accompanying geological constraints from the northern part of Danakil Depression, northernmost Ethiopia, reveal that a thick (<1-km) sequence of evaporites has been deposited over ~100,000 years in a basin that includes a major, east-dipping normal fault. The deposition of modern evaporites (i.e., URS) are characteristic of a salt pan environment, as opposed to marine-fed setting, with surface water depths not exceeding a few meters. The style of deformation in the Danakil basin, when considered in light of the region's markedly thinned crust, implies that the final stages of breakup in Ethiopia can be described best by an extension model dominated by ductile plate stretching and upper-crustal brittle faulting. The associated subsidence and basin formation is promoting the accumulation of thick sequences of evaporites, akin to those often observed at rifted passive margins

worldwide. Magma assisted rifting dominates extension elsewhere in Afar, but our observations from Danakil reveal that the subaerial onset of magmatic extension during rift development does not necessarily herald the onset of seafloor spreading.

Acknowledgments

I. B. acknowledges support from the National Research Council of Italy, which funded a visit to G. C. in Florence in May 2015. I. B. also acknowledges support from Leverhulme Trust grant RPG-2013-332. D. K. acknowledges support from the National Research Council of Italy, which funded a visit by D. K. to G. C. in Florence in June 2013. D. K. is supported by NERC grant NE/L013932/1. C. M. is funded by an Imperial College Research Fellowship. We thank Allana Potash Corporation for providing the data used in this study. University of Leeds acknowledges the support of Landmark Graphics Corporation via the Landmark University Grant Program, agreements 2001-COM-024982, 2008-CONT-010888, and subsequent renewals. We thank Claudio Faccenna for careful editorial handling, and Raphael Pik, Bernard Le Gall, and Balemwal Atnafu for insightful reviews. Data analyzed in this study are available from Allana Potash Corporation: <http://www.allanapotash.com>. For additional information concerning the geology of the Dallol area, the reader is directed to John Warren's blogs at www.saltworkconsultants.com.

References

- ArRajehi, A., McClusky, S., Reilinger, R., Daoud, M., Alchalbi, A., Ergintav, S., et al. (2010). Geodetic constraints on present-day motion of the Arabian Plate: Implications for Red Sea and Gulf of Aden rifting. *Tectonics*, 29, TC3011. <https://doi.org/10.1029/2009TC002482>
- Atnafu, B., Kidane, T., Foubert, A., Jaramillo-Vogel, D., Schaegis, J.-C., & Henriot, J.-P. (2015). Reading history in Afar. *EOS*, 96, 12–15.
- Ayele, A., Stuart, G., Bastow, I., & Keir, D. (2007). The August 2002 earthquake sequence in north Afar: Insights into the neotectonics of the Danakil microplate. *Journal of African Earth Sciences*, 48(2–3), 70–79. <https://doi.org/10.1016/j.jafrearsci.2006.06.011>
- Bannert, D., Brinckmann, J., Käding, K. C., Knetsch, G., Kürsten, M., & Mayrhofer, H. (1970). Zur Geologie der Danakil-Senke. *Geologische Rundschau*, 59, 409–443.
- Barberi, F., & Varet, J. (1977). Volcanism of Afar: Small-scale plate tectonics implications. *Geological Society of America Bulletin*, 88(9), 1251–1266.
- Bastow, I., & Keir, D. (2011). The protracted development of the continent-ocean transition in Afar. *Nature Geoscience*, 4(4), 248–250. <https://doi.org/10.1038/NNGEO01095>
- Bastow, I., Pilidou, S., Kendall, J.-M., & Stuart, G. (2010). Melt-induced seismic anisotropy and magma assisted rifting in Ethiopia: evidence from surface waves. *Geochemistry, Geophysics, Geosystems*, 11, Q0AB05. <https://doi.org/10.1029/2010GC003036>
- Billham, R., Bendick, R., Larson, K., Mohr, P., Braun, J., Tesfaye, S., & Asfaw, L. (1999). Secular and tidal strain across the Main Ethiopian Rift. *Geophysical Research Letters*, 26, 2789–2792. <https://doi.org/10.1029/1998GL005315>
- Bonatti, E., Emiliani, C., Ostlund, G., & Rydell, H. (1971). Final desiccation of the Afar rift, Ethiopia. *Science*, 172(3982), 468–469. <https://doi.org/10.1126/science.172.3982.468>
- Booth, A. D., Clark, R. A., & Murray, T. (2011). Influences on the resolution of GPR velocity analyses and a Monte Carlo simulation for establishing velocity precision. *Near Surface Geophysics*, 9(5), 399–411.
- Cornwell, D., Mackenzie, G., England, R., Maguire, P., Asfaw, L., & Oluma, B. (2006). Northern Main Ethiopian rift crustal structure from new high-precision gravity data, in the Afar Volcanic Province within the East African Rift System, eds. Yirgu, G., Ebinger, C.J. & Maguire, P.K.H. *Geological Society of London, Special Publication*, 256, 307–321.
- Corti, G., Agostini, A., Keir, D., Van Wijk, J., Bastow, I., & Ranalli, G. (2015). Magma-induced axial subsidence during final-stage rifting: Implications for the development of seaward-dipping reflectors. *Geosphere*, 11(3), 563–571. <https://doi.org/10.1130/GES01076.1>
- Daniels, K., Bastow, I., Keir, D., Sparks, R., & Menand, T. (2014). Thermal models of dyke intrusion during development of continent–ocean transition. *Earth and Planetary Science Letters*, 385, 145–153. <https://doi.org/10.1016/j.epsl.2013.09.018>
- Dumont, S., Socquet, A., Grandin, R., Doubre, C., & Klinger, Y. (2016). Surface displacements on faults triggered by slow magma transfers between dyke injections in the 2005–2010 rifting episode at Dabbahu-Manda-Hararo rift (Afar, Ethiopia). *Geophysical Journal International*, 204(1), 399–417. <https://doi.org/10.1093/gji/ggv449>
- Eagles, G., Gloaguen, R., & Ebinger, C. (2002). Kinematics of the Danakil microplate. *Earth and Planetary Science Letters*, 203, 607–620.
- Ebinger, C., Ayele, A., Keir, D., Rowland, J., Yirgu, G., Wright, T., et al. (2010). Length and timescales of rift faulting and magma intrusion: The Afar rifting cycle from 2005 to present. *Annual Review of Earth and Planetary Sciences*, 38(1), 439–466. <https://doi.org/10.1146/annurev-earth-040809-152333>
- Ebinger, C., & Casey, M. (2001). Continental breakup in magmatic provinces: An Ethiopian example. *Geology*, 29(6), 527–530. [https://doi.org/10.1130/0091-7613\(2001\)029<0527:CBIMPA>2.0.CO;2](https://doi.org/10.1130/0091-7613(2001)029<0527:CBIMPA>2.0.CO;2)
- Ebinger, C., & Hayward, N. (1996). Soft plates and hot spots: Views from Afar. *Journal of Geophysical Research*, 101, 21,859–21,876. <https://doi.org/10.1029/96JB02118>
- Ebinger, C. J., Keir, D., Bastow, I. D., Whaler, K., Hammond, J. O. S., Ayele, A., et al. (2017). Crustal structure of active deformation zones in Africa: Implications for global crustal processes. *Tectonics*, 36, 3298–3332. <https://doi.org/10.1002/2017TC004526>
- Field, L., Barnie, T., Blundy, J., Brooker, R., Keir, D., Lewi, E., & Saunders, K. (2012). Integrated field, satellite and petrological observations of the November 2010 eruption of Erta Ale. *Bulletin of Volcanology*, 74(10), 2251–2271. <https://doi.org/10.1007/s00445-012-0660-7>
- Foubert, A., Jaramillo-Vogel, D., Eisenhauer, A., Schaegis, J.-C., Atnafu, B., & Kidane, T. (2015a). Coral reefs and microbial deposits in an active rift setting: Insights from the Danakil Depression (Afar, Ethiopia). Abstract Book Bathurst Meeting 2015, Edinburgh, United Kingdom.
- Foubert, A., Jaramillo-Vogel, D., Eisenhauer, A., Schaegis, J.-C., Atnafu, B., & Kidane, T. (2015b). SERENA—Sedimentary record of the northern Afar (Ethiopia) coral reefs and microbial deposits in an active rift setting. 1st International Carbonate Mound Conference 2015, Monte Verita, Switzerland.
- Foubert, A., Kidane, T., Atnafu, B., & the ADD-ON ICDCP Team (2018). Stepping stones towards a unique archive in the Danakil Basin: Afar Dallol Drilling—ONset of sedimentary processes in an active rift basin (ADD-ON), *Geophysical Research Abstracts*, 20, EGU2018–18894.
- Fruehn, J., Fliedner, M., & White, R. (2001). Integrated wide-angle and near-vertical subbasalt study using large-aperture seismic data from the Faeroe-Shetland region. *Geophysics*, 66(5), 1340–1348. <https://doi.org/10.1190/1.1487079>
- Garland, C. (1980). Geology of the Adigrat area, Provisional Military Government of Socialist Ethiopia, Ministry of Mines, Energy & Water Resources, Geological Survey of Ethiopia.
- Grandin, R., Jacques, E., Nercessian, A., Ayele, A., Doubre, C., Socquet, A., et al. (2011). Seismicity during lateral dike propagation: insights from new data in the recent Manda Hararo-Dabbahu rifting episode (Afar, Ethiopia). *Geochemistry, Geophysics, Geosystems*, 12, Q0AB08. <https://doi.org/10.1029/2010GC003434>
- Hagos, M., Koeberl, C., & van Wyk de Vries, B. (2016). The Quaternary volcanic rocks of the northern Afar Depression (northern Ethiopia): Perspectives on petrology, geochemistry, and tectonics. *Journal of African Earth Sciences*, 117, 29–47. <https://doi.org/10.1016/j.jafrearsci.2015.11.022>
- Hammond, J., Kendall, J.-M., Stuart, G., Keir, D., Ebinger, C., Ayele, A., & Belachew, M. (2011). The nature of the crust beneath the Afar triple junction: Evidence from receiver functions. *Geochemistry, Geophysics, Geosystems*, 12, Q12004. <https://doi.org/10.1029/2011GC003738>
- Hayward, N., & Ebinger, C. (1996). Variations in the along-axis segmentation of the Afar rift system. *Tectonics*, 15, 244–257. <https://doi.org/10.1029/95TC02292>
- Hill, D. G. (1993). Multiple log potash assay. *Journal of Applied Geophysics*, 30(4), 281–295. [https://doi.org/10.1016/0926-9851\(93\)90037-Y](https://doi.org/10.1016/0926-9851(93)90037-Y)
- Holwerda, J. G., & Hutchinson, R. W. (1968). Potash-bearing evaporites in the Danakil area, Ethiopia. *Economic Geology*, 63, 124–150.

- Illsley-Kemp, F., Keir, D., Bull, J., Ayele, A., Hammond, J., Kendall, J.-M., et al. (2017). Local earthquake magnitude scale and b-value for the Danakil region of northern Afar. *Bulletin of the Seismological Society of America*, *107*(2), 521–531. <https://doi.org/10.1785/0120150253>
- Keir, D., Bastow, I., Corti, G., Mazzarini, F., & Rooney, T. (2015). The origin of along-rift variations in faulting and magmatism in the Ethiopian Rift. *Tectonics*, *34*, 464–477. <https://doi.org/10.1002/2014TC003698>
- Keir, D., Bastow, I. D., Pagli, C., & Chambers, E. (2013). The development of extension and magmatism in the Red Sea rift of Afar. *Tectonophysics*, *607*, 98–114. <https://doi.org/10.1016/j.tecto.2012.10.015>
- Keir, D., Pagli, C., Bastow, I., & Ayele, A. (2011). The magma-assisted removal of Arabia in Afar: Evidence from dike injection in the Ethiopian rift captured using InSAR and seismicity. *Tectonics*, *30*, TC2008. <https://doi.org/10.1029/2010TC002785>
- Kendall, J.-M., Pilidou, S., Keir, D., Bastow, I., Stuart, G., & Ayele, A. (2006). Mantle upwellings, melt migration and the rifting of Africa: Insights from seismic anisotropy, in the Afar Volcanic Province within the East African Rift System, eds. Yirgu, G. Ebinger, C.J. & Maguire, P.K.H. *Geological Society of London, Special Publication*, *259*, 271–293.
- Keranen, K., Klempner, S., Gloaguen, R., & EAGLE Working Group (2004). Three-dimensional seismic imaging of a protoridge axis in the main Ethiopian rift. *Geology*, *32*(11), 949–952. <https://doi.org/10.1130/G20737.1>
- Kogan, L., Fisseha, S., Bendick, R., Reilinger, R., McClusky, S., King, R., & Solomon, T. (2012). Lithospheric strength and strain localization in continental extension from observations of the East African Rift. *Journal of Geophysical Research*, *117*, B03402. <https://doi.org/10.1029/2011JB008516>
- Lalou, C., Nguyen, H., Faure, H., & Moreira, L. (1970). Datation par la méthode U/Th des hauts niveaux des coraux de la dépression de l'Afar (Ethiopie). *Revue de Géographie Physique et de Géologie Dynamique*, *12*, 3–8.
- Lascialfari, M. (2017). Quantifying the uncertainty of depth conversion for seismic reflection data from Ethiopia's Danakil Depression. University of Leeds, MSc Exploration Geophysics Thesis.
- Lewi, E., Keir, D., Birhanu, Y., Stuart, G., Wright, T., & Calais, E. (2016). Use of a high-precision gravity survey to understand the formation of oceanic crust and the role of melt at the southern Red Sea rift in Afar, Ethiopia. *Geological Society of London, Special Publication*, *420*(1), 165–180. <https://doi.org/10.1144/SP420.13>
- Mackenzie, G., Thybo, H., & Maguire, P. (2005). Crustal velocity structure across the Main Ethiopian Rift: Results from 2-dimensional wide-angle seismic modelling. *Geophysical Journal International*, *162*(3), 994–1006. <https://doi.org/10.1111/j.1365-246X.2005.02710.x>
- Magee, C., Bastow, I., van Wyk de Vries, B., Jackson, C., Hetherington, R., Hagos, M., & Hoggett, M. (2017). Structure and dynamics of surface uplift induced by incremental sill emplacement. *Geology*, *45*, 431–434. <https://doi.org/10.1130/G38839.1>
- Magee, C., Muirhead, J., Karvelas, A., Holford, S., Jackson, C., Bastow, I., et al. (2016). Lateral magma flow in mafic sill complexes. *Geosphere*, *12*(3), 809–841. <https://doi.org/10.1130/GES01256.1>
- Maguire, P., Keller, G., Klempner, S., Mackenzie, G., Harder, S., O'Reilly, B., et al. (2006). Crustal structure of the northern Main Ethiopian Rift from the EAGLE controlled-source survey; a snapshot of incipient lithospheric break-up, in the Afar Volcanic Province within the East African Rift System, eds. Yirgu, G. Ebinger, C.J. & Maguire, P.K.H. *Geological Society of London, Special Publication*, *259*, 271–293.
- Makris, J., & Ginzburg, A. (1987). The Afar Depression: Transition between continental rifting and sea floor spreading. *Tectonophysics*, *141*(1–3), 199–214. [https://doi.org/10.1016/0040-1951\(87\)90186-7](https://doi.org/10.1016/0040-1951(87)90186-7)
- McClusky, S., Reilinger, R., Ogubazghi, G., Amleson, A., Healebe, B., Vernant, P., et al. (2010). Kinematics of the southern Red Sea–Afar Triple Junction and implications for plate dynamics. *Geophysical Research Letters*, *37*, L05301. <https://doi.org/10.1029/2009GL041127>
- McDermott, K., & Reston, T. (2015). To see, or not to see? Rifted margin extension. *Geology*, *43*(11), 967–970. <https://doi.org/10.1130/G36982.1>
- Nobile, A., Pagli, C., Keir, D., Wright, T., Ayele, A., Ruch, J., & Acocella, V. (2012). Dike-fault interaction during the 2004 Dallol intrusion at the northern edge of the Erta Ale Ridge (Afar, Ethiopia). *Geophysical Research Letters*, *39*, L19305. <https://doi.org/10.1029/2012GL053152>
- Pagli, C., Wright, T., Ebinger, C., Yun, S., Cann, J., Barnie, T., & Ayele, A. (2012). Shallow axial magma chamber at the slow-spreading Erta Ale Ridge. *Nature Geoscience*, *5*(4), 284–288. <https://doi.org/10.1038/ngeo1414>
- Petersen, U., Andersen, M., & White, R. (2006). Seismic imaging of basalts at Glyvursnes, Faroe Islands: Hunting for future exploration methods in basalt covered areas. *First Break*, *24*(1093), 45–52. <https://doi.org/10.3997/1365-2397.2006006>
- Pickup, S. L. B., Whitmarsh, R. B., Fowler, C. M. R., & Reston, T. J. (1996). Insight into the nature of the ocean-continent transition off West Iberia from a deep multichannel seismic reflection profile. *Geology*, *24*(12), 1079–1082. [https://doi.org/10.1130/0091-7613\(1996\)024<1079:IITNOT>2.3.CO;2](https://doi.org/10.1130/0091-7613(1996)024<1079:IITNOT>2.3.CO;2)
- Pollard, D. D., & Johnson, A. M. (1973). Mechanics of growth of some laccolithic intrusions in the Henry Mountains, Utah, II: Bending and failure of overburden layers and sill formation. *Tectonophysics*, *18*, 311–354. [https://doi.org/10.1016/0040-1951\(73\)90051-6](https://doi.org/10.1016/0040-1951(73)90051-6)
- Ranero, C., & Pérez-Gussinyé, M. (2010). Sequential faulting explains the asymmetry and extension discrepancy of conjugate margins. *Nature*, *468*(7321), 294–299. <https://doi.org/10.1038/nature09520>
- Reading, H. (2009). *Sedimentary environments: Processes, facies and stratigraphy*. Oxford, UK: John Wiley & Sons.
- Reeve, M. T., Jackson, C. A.-L., Bell, R. E., Magee, C., & Bastow, I. D. (2016). The stratigraphic record of pre-breakup geodynamics: Evidence from the Barrow Delta, offshore Northwest Australia. *Tectonics*, *35*, 1935–1968. <https://doi.org/10.1002/2016TC004172>
- Reston, T., & McDermott, K. (2014). An assessment of the cause of the 'extension discrepancy' with reference to the west Galicia margin. *Basin Research*, *26*(1), 135–153. <https://doi.org/10.1111/bre.12042>
- Reston, T. J. (2009). The extension discrepancy and syn-rift subsidence deficit at rifted margins. *Petroleum Geoscience*, *15*(3), 217–237. <https://doi.org/10.1144/1354-079309-845>
- Rooney, T., Bastow, I., Keir, D., Mazzarini, F., Movsesian, E., Grosfils, E., et al. (2014). The protracted development of focused magmatic intrusion during continental rifting. *Tectonics*, *33*, 875–897. <https://doi.org/10.1002/2013TC003514>
- Rowland, J., Baker, E., Ebinger, C., Keir, D., Kidane, T., Biggs, J., et al. (2007). Fault growth at a nascent slow-spreading ridge: 2005 Dabbahu rifting episode, Afar. *Geophysical Journal International*, *171*(3), 1226–1246. <https://doi.org/10.1111/j.1365-246X.2007.03584.x>
- Rubin, A. M. (1992). Dike-induced faulting and graben subsidence in volcanic rift zones. *Journal of Geophysical Research*, *97*, 1839–1858.
- Ruch, J., Warren, J. K., Risacher, F., Walter, T. R., & Lanari, R. (2012). Salt lake deformation detected from space. *Earth and Planetary Science Letters*, *331–332*, 120–127.
- Siebert, L., Simkin, T., & Kimberly, P. (2010). *Volcanoes of the world* (3rd ed., p. 568). Berkeley: University of California Press.
- Stab, M., Bellahsen, N., Pik, R., Quidelleur, X., Ayalew, D., & Leroy, S. (2016). Modes of rifting in magma-rich settings: Tectono-magmatic evolution of central Afar. *Tectonics*, *35*, 2–38. <https://doi.org/10.1002/2015TC003893>
- Stuart, G., Bastow, I., & Ebinger, C. (2006). Crustal structure of the northern Main Ethiopian Rift from receiver function studies, in the Afar Volcanic Province within the East African Rift System, eds. Yirgu, G. Ebinger, C.J. & Maguire, P.K.H. *Geological Society of London, Special Publication*, *259*, 271–293.
- Symonds, P. A., Planke, S., Frey, O., & Skogseid, J. (1998). Volcanic evolution of the western Australian continental margin and its implications for basin development. *The Sedimentary Basins of Western Australia*, *2*, 33–54.

- Tesfaye, S., Harding, D., & Kusky, T. (2003). Early continental breakup boundary and migration of the Afar triple junction, Ethiopia. *Geological Society of America Bulletin*, *115*(9), 1053–1067.
- Vigny, C., Huchon, P., Ruegg, J., Khanbari, K., & Asfaw, L. (2006). Confirmation of Arabia plate slow motion by new GPS data in Yemen. *Journal of Geophysical Research*, *111*, B02402. <https://doi.org/10.1029/2004JB003229>
- Warren, J. K. (2016). *Evaporites: A compendium* (p. 1854). Berlin: Springer.
- Watts, A. B. (2001). *Isostasy and flexure of the lithosphere*. New York, Melbourne: Cambridge University Press.
- White, R., Smith, L., Roberts, A., Christie, P., Kuszniir, N., & the rest of the iSIMM Team (2008). Lower-crustal intrusion on the North Atlantic continental margin. *Nature*, *452*, 7186.
- Wolfenden, E., Ebinger, C., Yirgu, G., Renne, P., & Kelley, S. (2005). Evolution of a volcanic rifted margin: Southern Red Sea, Ethiopia. *Bulletin Geological Society of America*, *117*(7), 846–864. <https://doi.org/10.1130/B25516.1>
- Wright, T., Ebinger, C., Biggs, J., Ayele, A., Yirgu, G., Keir, D., & Stork, A. (2006). Magma-maintained rift segmentation at continental rapture in the 2005 Afar dyking episode. *Nature*, *442*(7100), 291–294. <https://doi.org/10.1038/nature04978>
- Ziolkowski, A., Hanssen, P., Gatliff, R., Jakubowicz, H., Dobson, A., Hampson, G., et al. (2003). Use of low frequencies for sub-basalt imaging. *Geophysical Prospecting*, *51*(3), 169–182. <https://doi.org/10.1046/j.1365-2478.2003.00363.x>